

# Fracture control on type, morphology and distribution of parasitic volcanic cones: An example from Mt. Etna, Italy

Claudia Corazzato <sup>a,\*</sup>, Alessandro Tibaldi <sup>a,b</sup>

<sup>a</sup> *Dipartimento di Scienze Geologiche e Geotecnologie, Università degli Studi di Milano-Bicocca Piazza della Scienza, 4-20126 Milano, Italy*

<sup>b</sup> *CNR-Istituto per la Dinamica dei Processi Ambientali, Milano, Italy*

Received 20 February 2005; accepted 10 April 2006

Available online 9 August 2006

## Abstract

This paper uses a coupled morphometric and stratigraphic analysis of several tens of parasitic pyroclastic cones of the SE flank of Mt. Etna volcano, Italy, to explain the structure of a poorly understood, actively deforming zone of the volcano. Moreover, we present a new general classification of pyroclastic cones based on the parameterisation of coeval eruption points along the same magma-feeding fracture. Each cone has been studied in detail in order to define its stratigraphic position, morphometric characteristics, growth evolution in relation to fracture distribution and orientation, stress field and morphology of the substratum. End members of this classification are at one side a simple, circular or elongated edifice that grew around a single eruption point and can be related to a magma-feeding fracture constrained by a relatively high confining stress in the substratum or a low magma pressure; the other end member is a multiple rifted, strongly elongated cone formed along multiple eruption points of a magma-feeding fracture constrained by a relatively low confining stress or a high magma pressure. Lithostratigraphic and historical analyses demonstrate that the cones in this area developed between 15 ka BP and historical times, the most recent one in 1669 AD, testifying to a high rate of lateral eruption occurrence in the area. These cones show N–S elongated maximum crater axes, N–S-trending axis of the depressed points of the crater rim, and southward and southeastward breaching directions, while coeval cones are N–S aligned. These morphometric characteristics reflect the geometry of N–S magma-feeding fractures. The area can be regarded as a transitional weakness zone between the N–S Rift and the releasing system represented by the transtensional Trecastagni and Mascalucia faults, indicating an E–W-oriented local component of extension possibly related to the interplay between the regional Timpe fault system and the eastward gravitational spreading of the volcano. The azimuth of breaching is controlled by magma-feeding fracture orientation and substrate morphology, especially in the eastern part of the area where it is influenced by the scarps related to the Timpe regional fault system, but it is also sensitive to cone development.

© 2006 Elsevier B.V. All rights reserved.

*Keywords:* Etna; monogenetic pyroclastic cones; scoria cones; morphometric analysis; magma-feeding fracture; Holocene

## 1. Introduction

In recent years, some authors have demonstrated that pyroclastic cones provide a great deal of geometric information that can help in distinguishing buried magma-feeding fractures (e.g. [Settle, 1979](#); [Pasquaré et al., 1988](#); [Tibaldi et al., 1989](#); [Ferrari and Tibaldi,](#)

\* Corresponding author. Tel.: +39 02 64484316; fax: +39 02 64484273.

E-mail address: [claudia.corazzato@unimib.it](mailto:claudia.corazzato@unimib.it) (C. Corazzato).

1991; Tibaldi, 1995). In this paper we refer to “magma-feeding fractures” as both pre-existing volcano-tectonic structures and propagating magma-filled cracks. In both cases, the orientation of these structures is related to the stress distribution in the substrate. These fractures act as avenues for the rise of magma during the time of eruption.

Using morphometric data of pyroclastic cones as an indirect method to reconstruct magma-feeding fractures can be particularly useful in areas where an extensive cover of volcanic and epiclastic deposits prevents the identification of structures of the volcanic substrate. Such a method allows the magma-feeding systems to be defined and the tectonic evolution of the region to be reconstructed. With the general term “substrate” we refer to the base on which a volcanic cone is emplaced, regardless of its size. For the

investigated pyroclastic cones, this term refers to the flank of the stratovolcano. On recent/active stratovolcanoes, the analysis of the morphometric character of parasitic cones can be the only method to identify volcano-tectonic structures affecting the flanks of the volcano. Some background is given by the observation that dykes propagate across the volcano parallel to the maximum horizontal compressional stress ( $\sigma_{Hmax}$ ), forming aligned parasitic cones (Nakamura, 1977). Similar arguments have been used to infer  $\sigma_{Hmax}$  from the alignment of volcanic centres (e.g. Johnson and Harrison, 1990; Strecker and Bosworth, 1991). Tibaldi (1995) introduced nine new morphometric parameters, giving emphasis to the use of morphological features of a single pyroclastic cone to infer the magma-feeding fracture geometry, rather than to the alignment of parasitic cones. Using cone alignment as sole basis

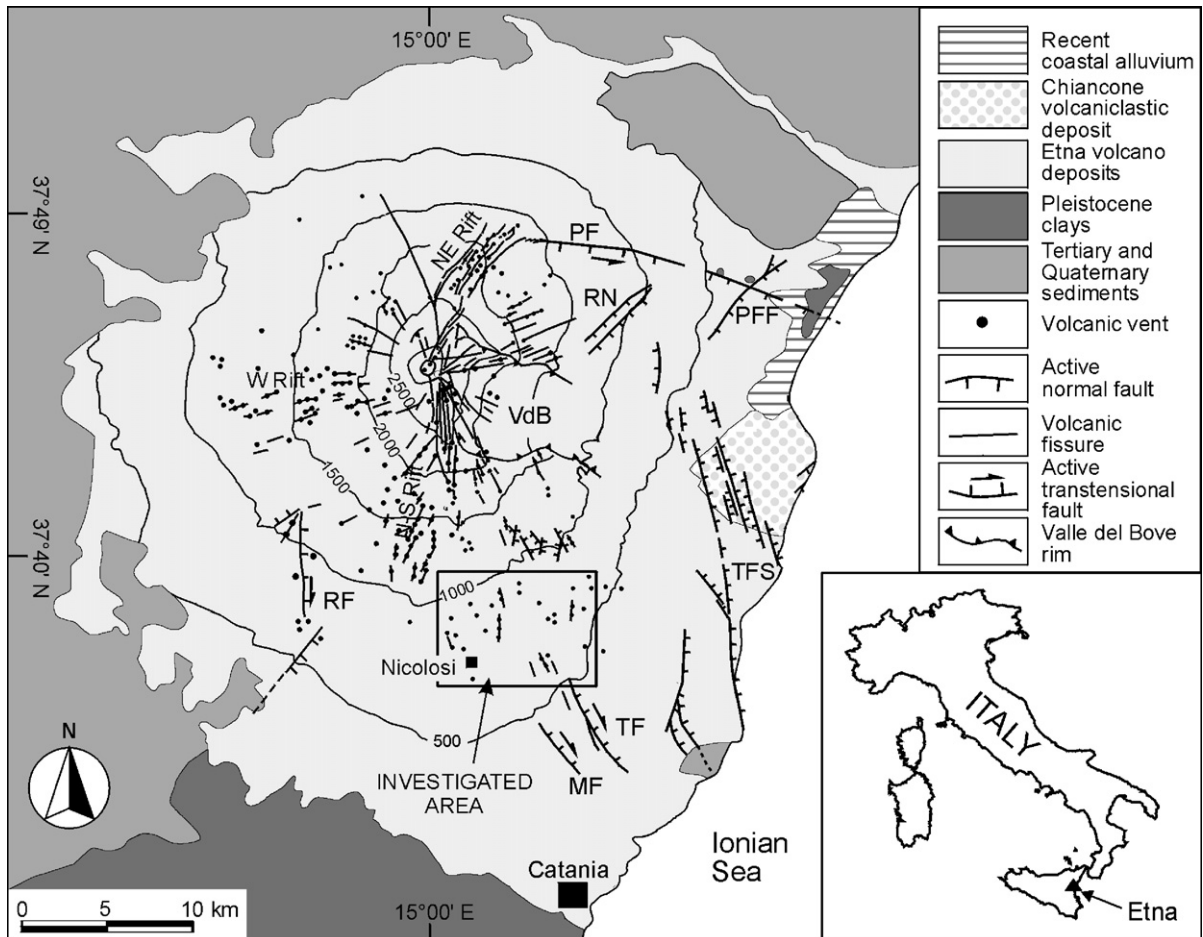


Fig. 1. General structural and geological sketch map of Mt. Etna, showing the distribution of parasitic pyroclastic cones on the volcano (modified after Tibaldi and Groppelli, 2002; Acocella and Neri, 2003; Azzaro, 2004; Branca et al., 2004; Bousquet and Lanzafame, 2004; Neri et al., 2004). The box locates the investigated area and Figs. 2B and 3A. VdB, Valle del Bove; TFS, Timpe Fault System; MF, Mascalucia Fault; TF, Trecastagni Fault; RF, Ragalna Fault; PF, Pernicana Fault; PFF, Piedimonte–Fiumefreddo Faults; RN, Ripe della Naca Faults.

can suffer from problems caused by the reliability of chosen points.

In this work, several tens of parasitic pyroclastic cones of the southeastern flank of Mt. Etna (Italy) (Figs. 1 and 2) were studied through the reconstruction of their stratigraphic position, geological and morphometric characteristics, and growth evolution in relation to the underlying magma-feeding fracture and substrate mor-

phology. These data were linked in order to constrain the factors controlling the emplacement of the parasitic cone, to locate the major weakness zones and to define their geometry.

At Mt. Etna, Settle (1979), Villari et al. (1988), Ferrari and Tibaldi (1991) and Mazzarini and Armienti (2001) studied the distribution of cones and some of their morphometric characteristics. All these works

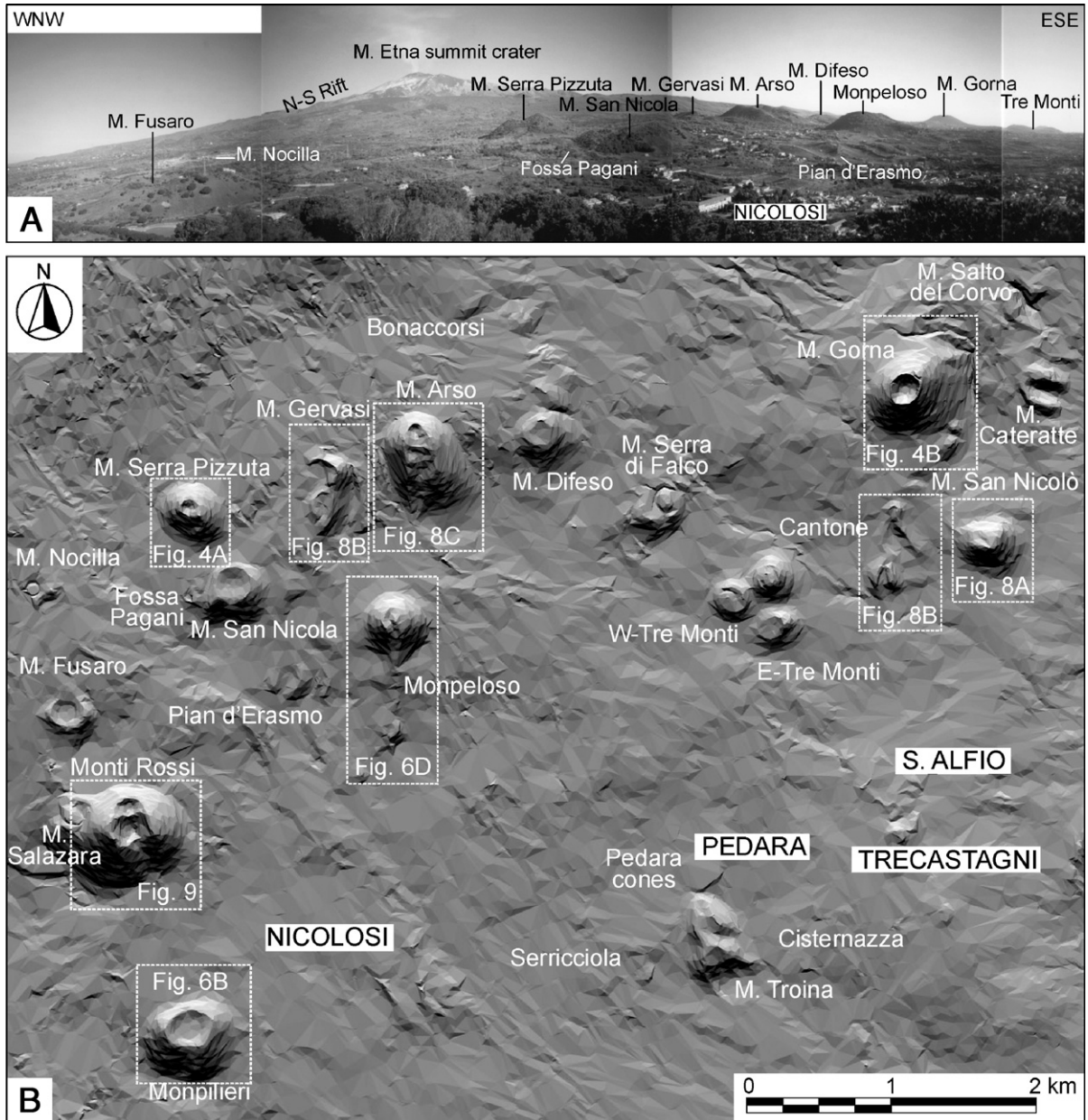


Fig. 2. (A) WNW–ESE-orientated panoramic view of the investigated area and the pyroclastic cones as it can be seen from Monti Rossi edifice. The view spans an extent of about 6 km. (B) Shaded view of the studied area (light from the N, digital elevation model after Pareschi et al., 1999), showing cone morphology and a gentle slope generally dipping to the SE, interrupted only in the eastern part of the area by an escarpment facing to the E–SE. Dashed boxes locate Figs. 4A,B, 6B,D, 8A,B,C and 9.

have a general approach, studying the entire population of secondary cones for delineating the main volcano-tectonic rift zones. This paper focuses on a poorly understood area where the extensive cover of lava flow, pyroclastic, debris and anthropogenic deposits prevents the reconstruction of the structural setting. This area is particularly important because it represents the “missing link” between the active N–S Rift, located in the upper part of Mt. Etna, and active southeastern coastal structures. Our study includes the reconstruction of the evolution of this part of Mt. Etna during the upper Pleistocene–Holocene. From a general point of view, our detailed analysis for each cone generates a new morphological classification of monogenetic cone types based on the parameterisation of coeval eruption points along the same magma-feeding fracture, and on their relationship with confining forces and magma pressure.

## 2. Geological and structural background

Mt. Etna is the largest active European stratovolcano, covering an area of about 1250 km<sup>2</sup> and reaching an elevation of 3340 m a.s.l. (Fig. 1). It is one of the most studied volcanoes since the first half of the nineteenth century. At its base lies the town of Catania and on its lower-middle flanks are several towns and villages with extensively cultivated areas.

The latest description of the Etnean volcanic stratigraphy is found in the Italian Geological Survey's 1:50,000 scale geological map (Foglio 625 Acireale, in press). It is the first of its kind, is derived from the work of several scientists in the last 15–20 years, and is fully based on modern stratigraphical concepts. An updated synthesis of the almost continuous evolution of Etnean volcanism is documented in Branca et al. (2004), where its history is subdivided in four main phases, ranging in time from about 580 ka BP up to Present. These, from the oldest to the youngest, are the: (i) Basal Tholeiitic; (ii) Timpe; (iii) Valle del Bove Centres; and (iv) Stratovolcano phases. The latest phase, which ranges in time from less than 60 ka to the Present, is defined by the construction of two different stratovolcanoes: Ellittico, which is mostly characterised by activity at the central vents; and Mongibello, whose products were erupted in the last 15 ka, covering a large part of the flanks of Mt. Etna following a summit caldera collapse of the Ellittico edifice. Mongibello is mainly characterised by effusive activity, represented by the products of summit and lateral vent eruptions, with the emplacement of monogenetic cones and large lava flows from vents located from 2800 to 400 m a.s.l. (Del

Carlo and Branca, 1998; Favalli et al., 1998). Products from strong explosive activity (plinian or subplinian) are also represented (Del Carlo et al., 2004; Branca and Del Carlo, 2005) and constitute marker levels invaluable for stratigraphic correlation. An example of this is the 122 BC plinian basaltic eruption that formed the Cratere del Piano, a 2-km wide summit caldera (Coltelli et al., 1998).

From a structural perspective, the volcanic edifice of Etna is characterised by the presence of the NE, N–S and W rift zones (McGuire and Pullen, 1989), located in the upper part of the volcano slopes. These rifts are characterised by a concentration of eruptive fissures, pyroclastic cones, and several main fault systems (Fig. 1). These fault systems are the Pernicana, Ragalna and the Mascalucia and Trecastagni faults. The Pernicana fault is on the NE flank and is a left-lateral strike-slip fault with a normal subordinate component (Tibaldi and Groppelli, 2002). Ragalna fault is on the SW flank and is a right-lateral strike-slip fault (dextral–normal motion, Rust and Neri, 1996). Mascalucia and Trecastagni (normal–dextral, Lo Giudice and Rasà, 1992; Froger et al., 2001) are on the southeastern sector and are also right-lateral strike-slip faults. Another main NNW-trending normal-fault system is represented by the Timpe, cutting the eastern flank of the volcano with downthrow to the east. The eastern flank of the volcano is undergoing active gravitational spreading towards the east (Borgia et al., 1992). This gravitational spreading is bounded by the Pernicana Fault system, the NE and N–S rift zones and the Mascalucia–Trecastagni fault system (e.g. Tibaldi and Groppelli, 2002). A proposed alternative structural boundary in place of the Mascalucia–Trecastagni fault system is the Ragalna fault. In the gravitational spreading model, this would involve an additional block moving more slowly (Rust and Neri, 1996; Neri et al., 2004) enhanced by subvolcanic magma accumulation and inflation (Borgia et al., 1992; Patané et al., 2003; Neri et al., 2004). The large Valle del Bove depression is the result of a series of lateral gravitational collapses occurring between 10 and 2 ka BP, which produced the Chiancone sequence of volcanoclastic deposits (Calvari et al., 2004; Fig. 1).

The studied area is on the southeastern slope of the volcano, from an altitude of 400 to 1100 m a.s.l. It includes the villages of Nicolosi, Pedara and Trecastagni, and has an areal extent of about 50 km<sup>2</sup> (Fig. 1). This area is entirely covered by the products of the Mongibello volcano, which is characterised by extensive lava flows and about 30 monogenetic pyroclastic cones made of bombs and lapilli layers, spatter ramparts extended along eruptive fissures, and some pyroclastic

fall deposits. The location is between the N–S Rift and the Mascalucia–Trecastagni fault system (Fig. 1).

### 3. Methodology

#### 3.1. Stratigraphy

A detailed geological survey at 1:10,000 scale of the study area was carried out based on lithostratigraphic criteria (Fig. 3A and B). The aim was to reconstruct the geological succession of volcanic products, in the framework of the general stratigraphic evolution of the volcano (Foglio 625 Acireale, *in press*). Emphasis was given to the relationship of each cone with its corresponding lava flow, where present (e.g. Fig. 4A), and the reconstruction of relative stratigraphic positions in the succession relative to other cones (e.g. Fig. 4B), based on direct and indirect stratigraphic correlations. Monogenetic cones being relatively small and scattered do not always have direct superposition of their products, while lava flows cover larger areas and allow relative dating (e.g. Fig. 4C). In this study, there are some uncertainties in relative ages because of the directional and confined emplacement of flows. The 122 BC plinian fall deposit (Coltelli et al., 1998), a dated stratigraphic marker, supplied absolute ages to the stratigraphic succession. Direct field observations complemented by data from the work of Del Carlo and Branca (1998), were used to distinguish cones that are younger or older than 122 BC.

The comparison of our data with the reports of historical eruptions (e.g. Romano and Sturiale, 1981, 1982; Chester et al., 1985 and cited references) provided further insights on the age of the cones. A very recent revision by Branca and Del Carlo (2004), in light of Foglio 625 Acireale (*in press*), reduced the number of reported historical eruptions which have corresponding deposits clearly documented stratigraphically.

Information on the relative ages of the cones were also obtained by applying the method proposed by Hasenaka and Carmichael (1985). This method classifies the stage of degradation of the edifice by means of morphological indices such as gully density and the surface morphology of associated lava flows. In this area, however, the method was often limited by strong anthropogenic modification of the landscape.

Our detailed geological survey enabled evaluation of the amount of cover at the base and lower slopes of the cones, improving the choice of parameters used for morphometric analysis. This was particularly important because in some areas, the emplacement of more recent lava flows, or in other cases pyroclastic deposits,

obscured the original shape of the cone base. The lack of such geological information could lead to inaccurate results.

#### 3.2. Morphometric analysis

A detailed morphometric field survey of each cone was performed. This led to the distinction of morphologies unresolved by 1:10,000 topographic maps and 1:12,500 aerial photographs. The morphology of the volcano slope was also analysed using 1:10,000 topographic maps, and shaded views of a DEM (Fig. 2) under different light orientations (Favalli et al., 1998; Pareschi et al., 1999).

Among the numerous morphometric features and parameters proposed by different authors (e.g. Porter, 1972; Settle, 1979; Wood, 1980; Hasenaka and Carmichael, 1985) regarding the absolute dimensions and dimension ratios of the cones, and the nine parameters advanced by Tibaldi (1995) that are more directly linked with fractures and tectonics, only those parameters useful for inferring the geometry of the magma-feeding fracture were chosen and measured (Table 1). Furthermore, the extended cover by more recent volcanic products masked the base of the monogenetic cones. This prevented the measurement of certain parameters and was not taken into account.

Morphometric measurements of pyroclastic cones were performed together with an estimate of substrate inclination. Previous studies (Tibaldi, 1995) have shown that the morphology of pyroclastic cones grown on horizontal or subhorizontal substrate topography ( $<9^\circ$ ) is not influenced by the effects of gravity along the slope.

Based on the above considerations, morphometric parameters that were taken into account mostly relate to craters and their features. In this work, only craters have been considered because they mimic the shape of the cone base (Tibaldi, 1995). Unlike the cone base, however, craters are usually not influenced or obscured by recent lava flows making them unrepresentative of the actual cone's ellipticity.

Measurements followed the criteria listed below:

- (1) Minimum and maximum crater diameters (Table 1) are used for calculating the degree of ellipticity. Only craters that present an almost continuous rim are measured. Those interrupted by breaching, or fissure-like, are not considered.
- (2) The degree of crater ellipticity is expressed as the ratio between the minimum and maximum crater diameter. A value of 1 represents a perfectly circular crater while values less than 1 represents

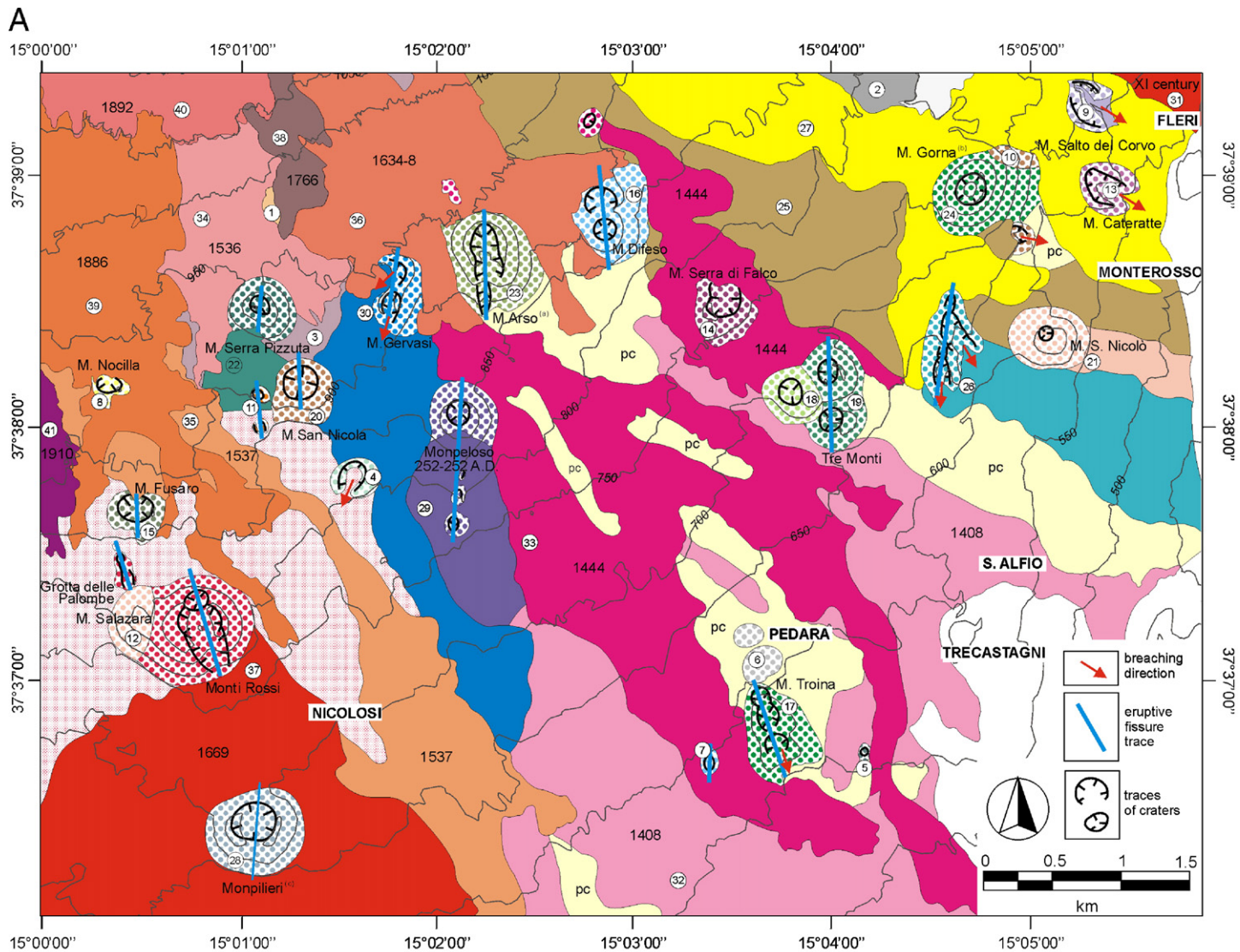


Fig. 3. (A) Simplified geological map of the studied area, from an original lithostratigraphic survey at 1:10,000 scale. Location in Fig. 1. Breaching directions and traces of inferred magma-feeding fractures are also indicated. (B) Stratigraphic sketch of the relationship between the various lithostratigraphic units (at the lava-flow rank) recognised in the studied area. Main marker levels are indicated, as well as the setting among UBSU and lithostratigraphic units of higher order as defined in Foglio 625 Acireale (in press). In brackets are reported corresponding historical eruptions according to Romano and Sturiale (1982) and Chester et al. (1985), although only the Monpeloso eruption age (252–253 AD) is confirmed by the recent work by Branca and Del Carlo (2004). (a) 425–424 BC, (b) 394 or 396 BC, (c) 693 BC, but post-122 according to Branca and Del Carlo (2004).

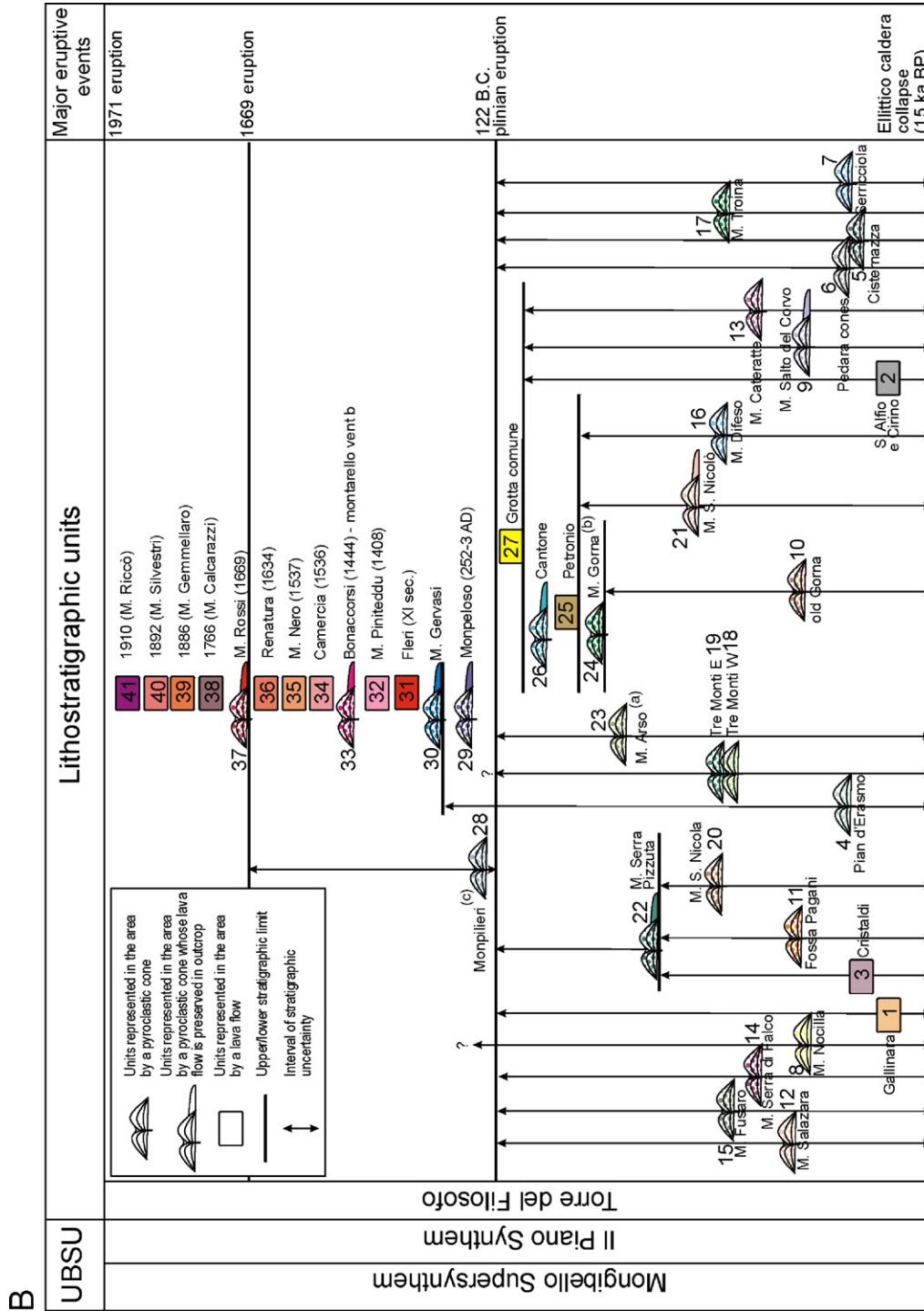


Fig. 3 (continued).

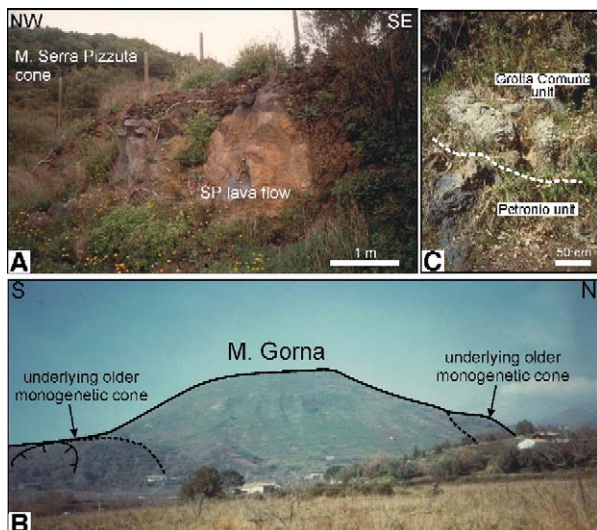


Fig. 4. Field examples of observed stratigraphic relationships. (A) M. Serra Pizzuta cone and associated lava flow outcrop. (B) M. Gorna cone and underlying older monogenetic edifices. (C) Stratigraphic relationship of two lava flows belonging to different lithostratigraphic units (Petronio and Grotta Comune units).

elliptical crater rims (Fig. 5). The percentage of circular crater rims versus the entire population gives a statistical weight for the analysis performed on elongated ones (Tibaldi, 1995). Although circular craters do not provide information related to elongation, they are useful for the analysis, if crater-rim depressed points (see number 4 below), or vent alignments (see number 5 below) are present.

- (3) Maximum crater elongation axis direction is expressed in terms of azimuth. The crater elongation is parallel to the geometry of the underlying magma-feeding fracture (Fig. 6A).
- (4) Crater-rim depressed points are considered parallel to the feeding-fracture geometry in the substrate (Fig. 6A). In a completely developed pyroclastic cone, the presence of elevated and depressed points in the crater rim represents the equivalent of the scoria rampart in the inception stage of Strombolian activity. The scoria rampart is normally parallel to the eruption fissure. This feature can also be present in perfectly circular cones. The strike of the line connecting the depressed points is expressed as an azimuth.
- (5) Alignments of the centre points of coeval craters (Fig. 6A) occur along the magma-feeding fracture. Cones usually develop one after the other with an upward propagation along the eruptive fissure until the fissure is sutured (Ollier, 1988). On the

basis of the stratigraphic reconstruction, the strike of these coeval alignments can be measured.

- (6) Breaching azimuth is the angle of downslope direction of the bisector of the collapse amphitheatre, and is measured clockwise from the north (Fig. 7C). Breaching results in a horseshoe-shaped depression left by collapse of the cone flank during or after its growth. In general, breaching is often associated with a lava flow (Fig. 7A and B). This phenomenon can be caused by gradual erosion and lowering of the cone flank due to a lava flow pouring out from the crater, or by lateral emission of the lava flow from the conduit into the cone flank that consequently collapses by undermining (Tibaldi, 1995). Breaching coincides with the weakest zone of the cone or with the direction of maximum stress applied to its flanks by magma bulging or fracture propagation. Such breaches are parallel to the geometry of the magma-feeding fracture (Fig. 7A) unless the cone is emplaced over a dipping substrate (Fig. 7B). The percentage of cones with breached craters relative to the entire cone population provides the statistical weight of this feature in the analysis.

## 4. Data and results

### 4.1. Stratigraphy of the area

The stratigraphic results are presented in the geological map of the studied area (Fig. 3A) and the stratigraphic sketch (Fig. 3B). Detailed fieldwork enabled the distinction of 41 lithostratigraphic units of “lava flow” rank, represented by different lava flows and monogenetic cones. The mainly historical lava flows originating at higher elevations north of the studied area have a significant areal extent. These flow deposits cover the substrate and lower slopes of most of the cones (Fig. 3A). Lava flows were emplaced following the maximum (although still gentle) slope-dip towards the SE and ESE. Several direct stratigraphic relationships between cones and lava flows were recognised and represented by horizontal lines in the stratigraphic sketch (Fig. 3B). Based on field evidence of the presence of the 122 BC fall-deposit marker level on the cone slopes or in the craters, and on published data (Del Carlo and Branca, 1998), the cones were subdivided into the pre- and post-122 BC periods. The stratigraphic position of some of the pre-122 BC scoria cones, however, still remains uncertain because the cone base and the associated lava flow are completely covered by historical lava flow deposits. Intervals of

Table 1  
Input data for the morphometric analysis

| Cone name              | Cone type <sup>(a)</sup> | Max crater diameter | Min crater diameter | Crater ellipticity ratio (min/max diameter) | Max crater elongation axis <sup>(d)</sup> | Coeval crater alignment <sup>(d)</sup> | Crater rim depressed points alignment <sup>(d)</sup> | Breaching bisector <sup>(d)</sup> |
|------------------------|--------------------------|---------------------|---------------------|---|---|--|--|-----------------------------------|
|                        |                          | (m)                 | (m)                 |   | (deg)                                     | (deg)                                  | (deg)  | (deg)                             |
| M. Fusaro (15)         | 1                        | 250                 | 190                 | 0.76  | 90  | –                                      | 178  | –                                 |
| M. Nocilla (8)         | 1                        | 180                 | 120                 | 0.67  | 88  | –                                      | 171  | –                                 |
| Monti Rossi (37)       | 5                        | (c)                 | (c)                 | –   | –   | 160                                    | –  | –                                 |
| Gr. Palombe (37)       | 3                        | (c)                 | (c)                 | –   | –   | 170                                    | –  | –                                 |
| M. Serra Pizzuta (22)  | 1                        | 160                 | 120                 | 0.75  | 160                                       | –                                      | 185  | –                                 |
| Monpilieri (28)        | 1                        | 350                 | 280                 | 0.80  | 245                                       | –                                      | 180  | –                                 |
| M. San Nicola (20)     | 1                        | 260                 | 260                 | 1.00  | –   | –                                      | 178  | –                                 |
| Fossa Pagani (11)      | N 1-a                    | 80                  | 70                  | 0.88  | 100                                       | 174                                    | –  | –                                 |
|                        | S                        | (f)                 | (f)                 | –   | –   | –                                      | 169  | –                                 |
| Pian d'Erasmus (4)     | 1                        | (b)                 | (b)                 | –   | –   | –                                      | –  | 203                               |
| Monpeloso (29)         | N 1-a                    | 160                 | 150                 | 0.94  | 182                                       | 3                                      | 185  | –                                 |
|                        | S                        | 110                 | 70                  | 0.64  | 186                                       | –                                      | –  | –                                 |
| M. Gervasi (30)        | N 2                      | (b)                 | (b)                 | –   | –   | 5                                      | –  | 240                               |
|                        | S                        | (b)                 | (b)                 | –   | –   | –                                      | –  | 195                               |
| M. Arso (23)           | 5                        | (c)                 | (c)                 | –   | –   | 178                                    | –  | –                                 |
| Serra di Falco (14)    | 1                        | 250                 | 250                 | 1.00  | –   | –                                      | –  | –                                 |
| E-Tre Monti (19)       | N 2                      | 180                 | 130                 | 0.72  | 186                                       | 178                                    | –  | –                                 |
|                        | S                        | 160                 | 150                 | 0.94  | 198                                       | –                                      | –  | –                                 |
| W-Tre Monti (18)       | 1                        | 190                 | 170                 | 0.89  | 170                                       | –                                      | –  | –                                 |
| M. Difeso (16)         | N 2                      | (b)                 | (b)                 | –   | –   | 175                                    | –  | –                                 |
|                        | S                        | 180                 | 180                 | 1.00  | –   | –                                      | –  | –                                 |
| M. Gorna (24)          | 1                        | 250                 | 220                 | 0.88  | 212                                       | –                                      | 148  | –                                 |
| NE-old Gorna (10)      | 1                        | (e)                 | (e)                 | –   | –   | –                                      | –  | –                                 |
| SE-old Gorna (10)      | 1                        | (b)                 | (b)                 | –   | –   | –                                      | –  | 102                               |
| Cantone (26)           | N 3                      | (b)                 | (b)                 | –   | –   | 186                                    | –  | 160                               |
|                        | S                        | (b)                 | (b)                 | –   | –   | –                                      | –  | 170                               |
| M. San Nicolò (21)     | 1                        | 100                 | 100                 | 1.00  | –   | –                                      | –  | –                                 |
| M. Cateratte (13)      | 1                        | (b)                 | (b)                 | –   | –   | –                                      | –  | 135                               |
| M. Salto del Corvo (9) | 1                        | (b)                 | (b)                 | –   | –   | –                                      | –  | 135                               |
| M. Troina (17)         | 4                        | (b)                 | (b)                 | –   | –   | 165                                    | –  | 160                               |
| Pedara cones (6)       | 1-a                      | (e)                 | (e)                 | –   | –   | –                                      | –  | –                                 |
| Bonaccorsi (37)        | 1                        | 110                 | 75                  | 0.68  | 190                                       | –                                      | –  | –                                 |
| Serricciola (7)        | 1                        | 100                 | 70                  | 0.70  | 187                                       | –                                      | –  | –                                 |
| Cisternazza (5)        | 1                        | 50                  | 40                  | 0.80  | 190                                       | –                                      | –  | –                                 |
| M. Salazara (12)       | (e)                      | (e)                 | (e)                 | –   | –   | –                                      | –  | –                                 |

(a) 1: simple cone; 1-a: alignment of simple cones; 2: multiple superimposed cone; 3: multiple coalescent cone; 4: mixed-type cone; 5: multiple rifted cone. (b) Breached crater. (c) Fissure-like crater. (d) Expressed as azimuth. (e) Crater not visible. (f) Rampart.

stratigraphic uncertainty are expressed as vertical double-headed arrows. The relative ages of some cones were evaluated based on the degradation stage of the edifices. Historical eruptions were considered in Fig. 3B following Chester et al. (1985) and Romano and Sturiale (1981, 1982), but after the general revision of the tephrostratigraphic record by Branca and Del Carlo (2004), only the Monpeloso cones and lava flows related to a Roman-age eruption was confirmed.

The lithostratigraphic units presented refer to the higher rank Torre del Filosofo lithostratigraphic unit, recently defined in Foglio 625 Acireale (in press), and to the Il Piano Synthem. This Unconformity Bounded Stratigraphic Unit represents the products of the most

recent edifice of the volcano, following the Ellittico summit caldera collapse event. The products of the studied area are all younger than 15 ka, with eleven lava flows and at least eight monogenetic cones that are historical in age (Fig. 3B). This is testimony to the high rate of occurrence of lateral eruptions and high number of pyroclastic cones per surface unit area (about one edifice every 2 km<sup>2</sup>).

#### 4.2. Cone types

Various types of monogenetic scoria cones were classified into five categories based on the parameterization of coeval eruption points along the same magma-

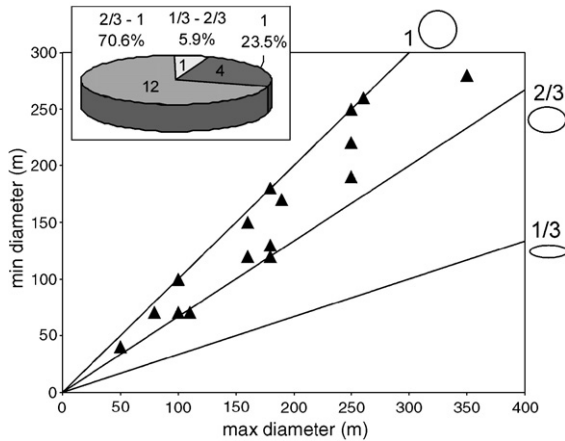


Fig. 5. Ellipticity plot (ratio between minimum and maximum crater diameters) for craters without breaching, and relative percentage for different classes of this ratio (inset diagram). Only a minority of the craters are perfectly circular (ratio equal to 1, 23.5%), while the majority of them are elliptical (ratio between 1 and 2/3, 70.6%, between 2/3 and 1/3, 5.9%) and provide useful information on the orientation of the feeding fracture.

feeding fracture. Because of the detailed lithostratigraphic survey performed in an area with a high density of scoria cones, a new classification scheme can be proposed with the following categories: (1) simple cones; (2) multiple superimposed cones; (3) multiple coalescent cones; (4) mixed-type cones; and (5) multiple rifted cones.

- (1) *Simple cones* are characterized by a unique vent and crater. The cone shape in plan view is extremely variable, from perfectly circular to markedly elliptical (Fig. 8A), and the dimensions of the cone can vary from tens to hundreds of metres. Most of the edifices studied can be ascribed to this type (Table 1), such as M. Nocilla, M. Fusaro, Monpilieri, M. Serra Pizzuta, M. San Nicola, M. Serra di Falco, M. Gorna, M. San Nicolò (Fig. 8A), Pian d'Erasmus and Serriciola cones. Some of the cones of this type have been affected by breaching (M. Cateratte, M. Serra di Falco, Pian d'Erasmus, Fig. 3A). This type also includes those distinct cones that developed contemporaneously along an eruptive fissure without reaching large dimensions, such as the “bottoniere” (rows of buttons, in Italian) (1-a, Table 1). In this case, simple cones usually develop one after the other with an upward propagation along the eruptive fissure until the fissure is sutured (Ollier, 1988). Examples are the

alignments of Monpeloso together with the smaller Grottalunga cones (Fig. 3A, Fig. 6D) that formed during the same eruptive event along a NS-striking fracture, and those of Fossa Pagani. Type (1) also includes rampart edifices such as the one located at Fossa Pagani (Fig. 3A).

- (2) *Multiple superimposed cones* are represented by overlapping cones related to the same eruption where craters are aligned but do not interfere with each other. The cone shape in plan view is usually strongly elliptical (Fig. 8B). Examples are M. Difeso (Fig. 3A) and M. Gervasi (Fig. 8B).
- (3) *Multiple coalescent cones* are given by superimposed edifices related to the same eruptive phase where craters interfere with each other (Fig. 3A). The cone shape in plan view is usually elliptical. The succession of crater development can often be reconstructed based on intersection criteria. An example is the Cantone edifice (Fig. 8B).
- (4) *Mixed-type cones* are characterized by features of both types 2 and 3 cones at the same monogenetic edifice. This is the case in M. Troina (Fig. 3A), where the southern part is composed of superimposed craters (type 2) and the northern part by coalescent craters (type 3).
- (5) *Multiple rifted cones* are strongly elongated monogenetic edifices which usually have large dimensions (hundreds of metres). They develop along magma-feeding fractures and maintain a markedly linear crater crossing one or two opposing flanks (Fig. 6C, Fig. 8C). These cones can't be misinterpreted as breached because the depression shows preserved primary geometry and spatter deposits. In the case of breaching, the original geometry of the layered volcanic products is cut by the collapse amphitheatre. Examples of this cone type in the area are the two large edifices of M. Arso (Fig. 6C, Fig. 8C) and Monti Rossi (Fig. 3A and Fig. 9).

#### 4.3. Morphometric data for reconstructing fracture geometry

When performing morphometric analysis on pyroclastic cones, it is also important to evaluate the morphological characteristics of the substrate, particularly changes in slope inclination. The area studied is generally characterized by a gentle slope with an average inclination ranging between 2° and 6° (Fig. 2A, B; Fig. 3A), dipping to the SSE and SE in the western and central parts of the area. This is also

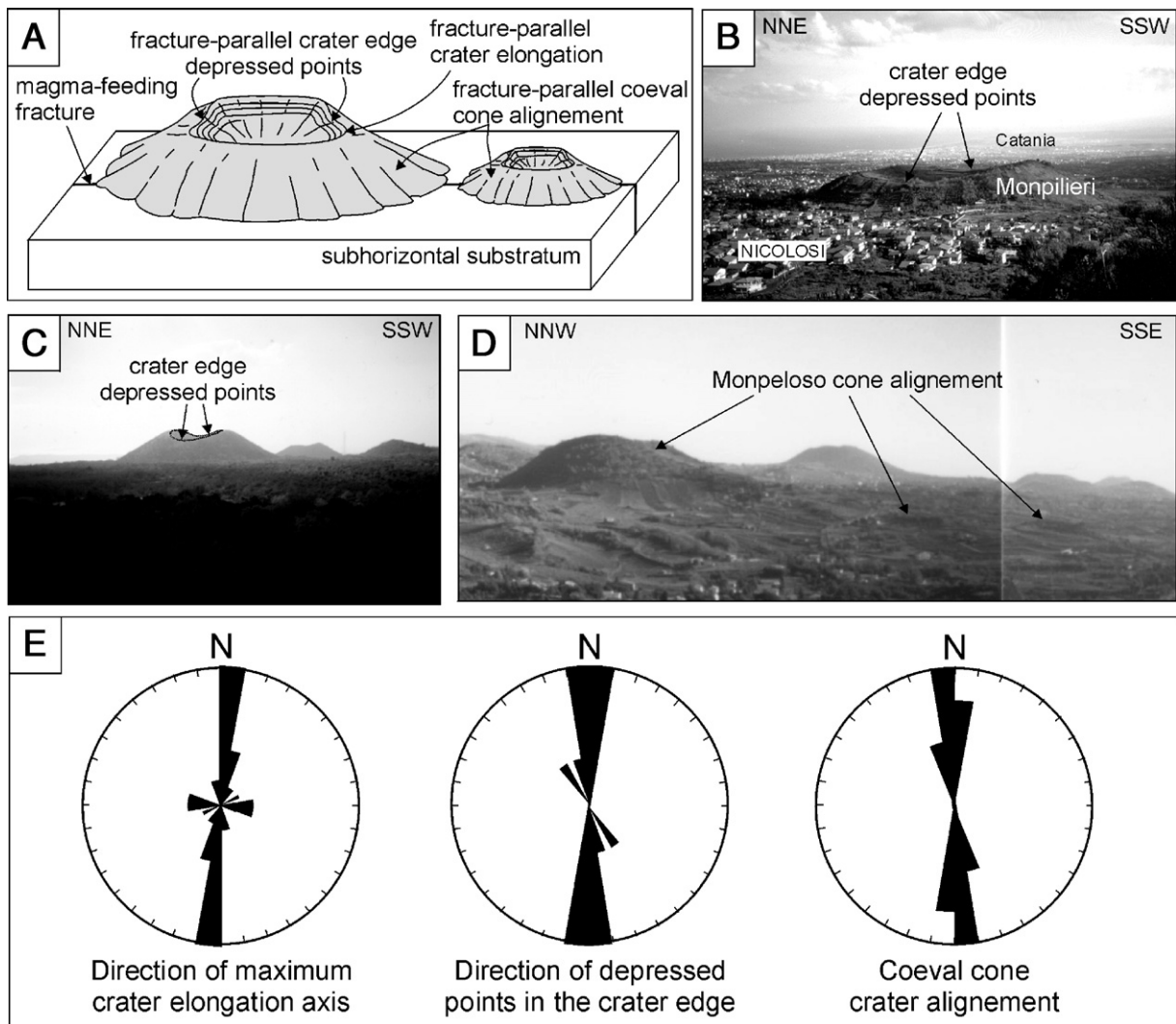


Fig. 6. (A) 3-D sketch of the measured morphometric characteristics of pyroclastic cones and their relationship with the orientation of the underlying feeding fracture (modified after Tibaldi, 1995): fracture-parallel crater elongation, crater rim depressed points, coeval cone alignment. (B) Monpilieri edifice and crater-rim depressed points striking N–S. (C) Some of the cones viewed from the north, showing the depressed points in the crater rim. (D) Monpeloso, an example of coeval cone alignment. (E) Rose diagrams related to the trend of: (i) maximum crater elongation axis, (ii) line connecting the depressed points in the crater rim, (iii) coeval cone crater alignment, expressed as an azimuth and represented as strike in intervals of  $10^\circ$ . The length of each leaf is proportional to the number of measurements. All these diagrams are concordant and show a N–S direction  $\pm 15^\circ$ .

indicated by the direction followed by lava flows. The dip azimuth gradually rotates in the eastern part where it dips to the east. In the northeastern sector, there is an appreciable increase in inclination (up to about  $20^\circ$  east of M. Gorna) with the presence of a morphological scarp towards the east (Fig. 3A). In the northern part, a moderate increase in the inclination of the topography is given by the presence of thick historical lava flows covering a significant part of M. Gervasi, M. Arso and M. Difeso's northern flanks.

#### 4.3.1. Ellipticity

In evaluating cone ellipticity only those cones that still keep an intact crater rim were considered. Coalesced, fissure-like or breached crater rims were not taken into account (Table 1).

Crater maximum diameters range between 50 and 350 m, while minimum diameters range between 40 and 280 m. Fig. 5 shows that only 4 out of the 17 craters considered (23.5%) are circular in plan view (ellipticity ratio equal to 1.0), whereas the others (76%) have a

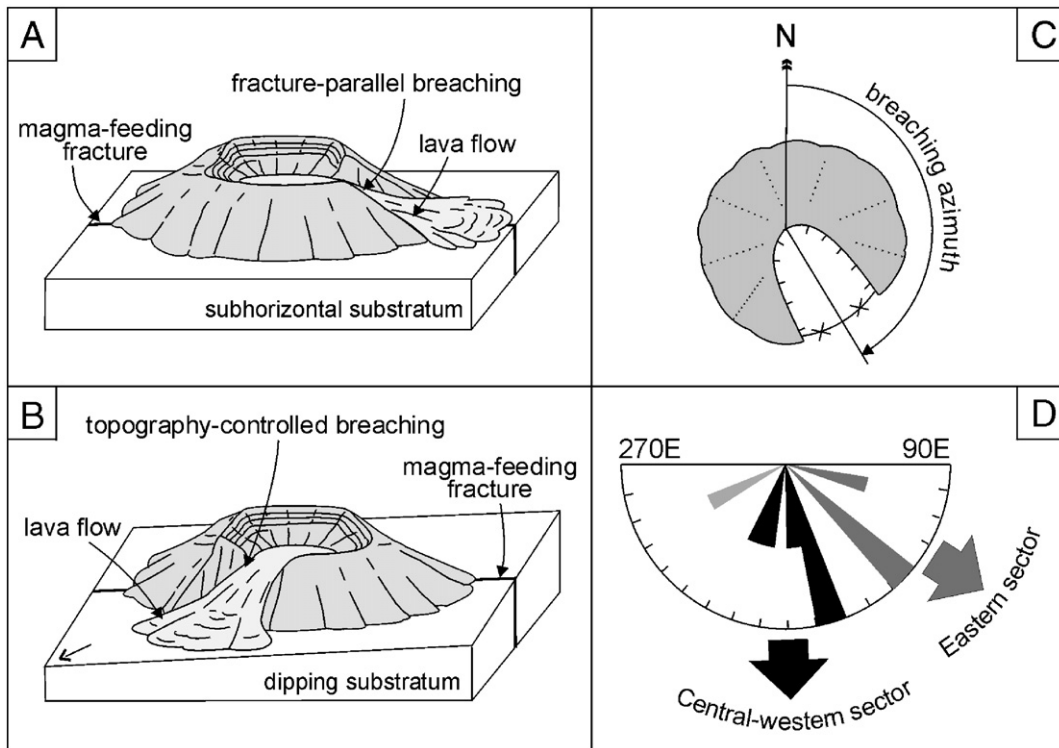


Fig. 7. About 27% of the cones studied exhibit breaching, and in some cases more than one crater is affected by this morphological feature. (A) In the case of a subhorizontal substrate (slope  $< 10^\circ$ ), breaching occurs parallel to the magma-feeding fracture that controls it (Tibaldi, 1995), while (B) in the case of a dipping substrate ( $> 10^\circ$ ), topography controls breaching orientation, regardless of the fracture geometry. (C) Breaching bisector azimuth is defined as the horizontal angle of direction measured clockwise from north. (D) Rose diagram of breaching bisector azimuth measured for the studied cones: in the central and western sector, where slope inclination is low, breaching is oriented dominantly southwards  $\pm 20^\circ$  — in agreement with the other morphometric parameters that suggest N–S-striking fractures. In the northeastern sector the slope has an inclination up to  $20^\circ$  and controls breaching direction, which is mainly to the SE ( $\pm 15^\circ$ ). The poorly represented WSW and ESE directions are due to local control by already formed portions of the same multiple edifice.

moderately elliptical shape, mainly falling in the range between 1 and 2/3 (ratio between 0.94 and 0.64). In addition, some of the circular craters provided useful information on the magma-feeding fracture geometry through the position of depressed points in the crater rim, or coeval alignments of craters (e.g. Monpeloso).

#### 4.3.2. Crater elongation, crater-rim depressed points, and alignment of coeval craters

The measured features that were used to infer the geometry of the magma-feeding fractures refer mainly to the character of single edifices and to aligned coeval cones (Fig. 6A). These features comprise: (1) the directions of the maximum crater-elongation axes of elliptical craters; (2) the strike of the line connecting depressed points in the crater rim (present in 8 cases); and (3) the strike of aligned coeval vents, including centres of craters in multiple superimposed or coalescent cones, fracture-like craters, or aligned coeval cones (Table 1).

In Fig. 6B and Fig. 6C two examples of crater-rim depressed points are presented. Fig. 6D shows the alignment of the Monpeloso coeval cones. The rose diagrams of Fig. 6E show the trend of these morphometric features. These data are concordant and show a dominant N–S trend ( $\pm 15^\circ$ ). Only a couple of measurements differ from this general trend, and basically relates to the diagram representing crater elongation. Nonetheless, this deviant trend is not reflected in the diagram of crater-rim depressed points because E–W elongated craters also show N–S aligned depressed points, as in the case of the Monpilieri cone (Fig. 6B).

#### 4.3.3. Breaching

The breaching depression is one of the most evident morphological features of the monogenetic cones studied, affecting 27% of the cone population. Examples of simple cones with breached craters are Pian d'Erasmus, M. Cateratte or M. Salto del Corvo, while multiple superimposed or coalescent edifices often show

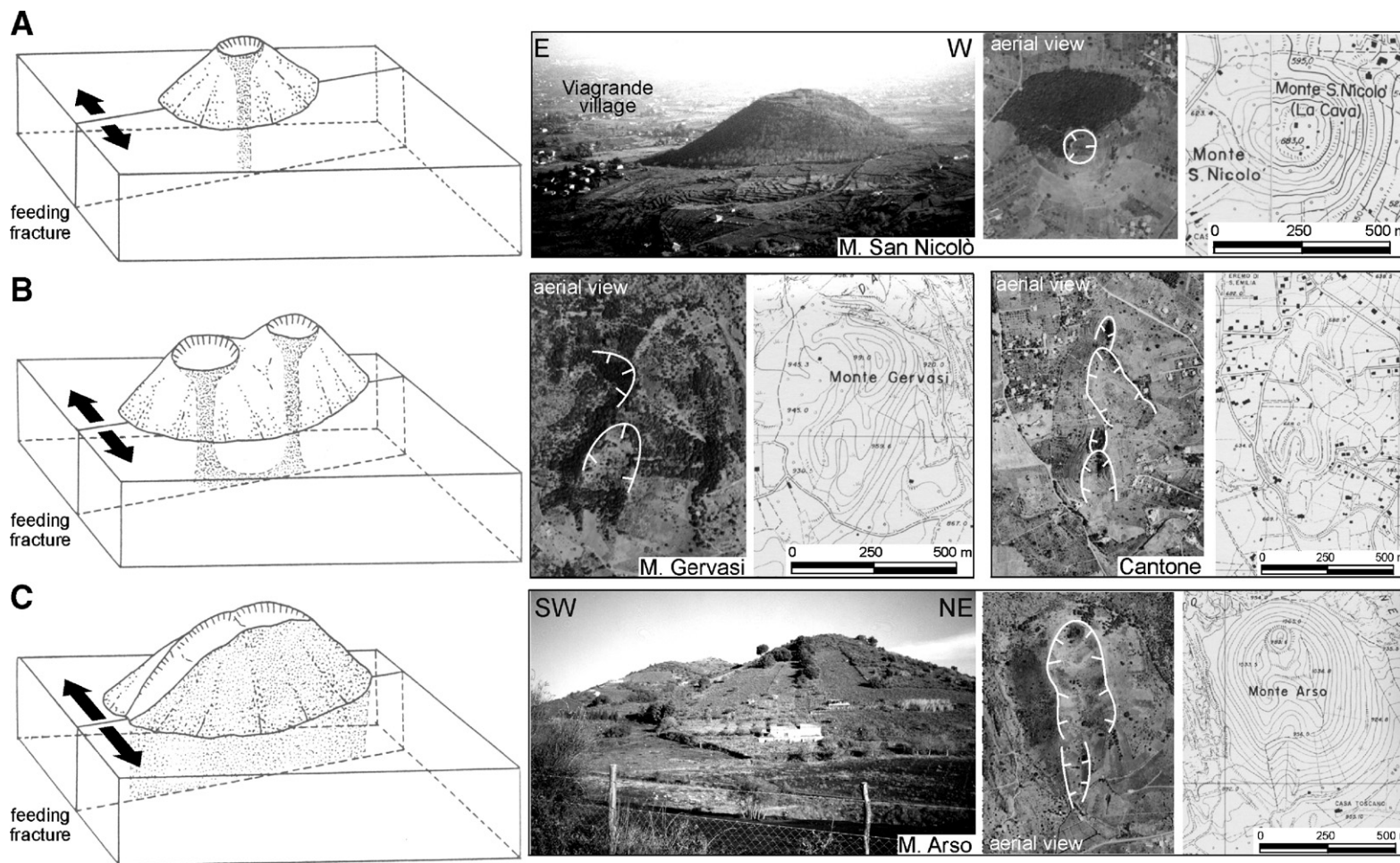


Fig. 8. New classification based on the parameterisation of the coeval eruption points along the same magma-feeding fracture, and the relationship of the resulting cone typologies with the confining forces and magma supply pressure. For each case, a general sketch and field examples are reported.

- (A). Simple cone (type 1), circular or elongated, that grew around a single eruption point and that can be related to a feeding fracture constrained by relatively high stress in the substrate or a low magma pressure. As an example of this typology, photo, aerial view and topographic map of M. San Nicolò cone are reported.
- (B). Multiple superimposed cone (type 2), in the case of two distinct crater openings. An example is represented by the M. Gervasi edifice. When craters coalesce, the cone type is defined as “multiple coalescent” (type 3, not shown), and an example is the Cantone edifice. Intermediate cases are represented by mixed-type (type 4, not shown).
- (C). Multiple rifted cone (type 5), strongly elongated and usually of large dimensions, formed along multiple eruption points of a feeding fracture constrained by a relatively low confining stress or a high magma pressure. The example of M. Arso (photo, aerial view and topographic map) is reported.

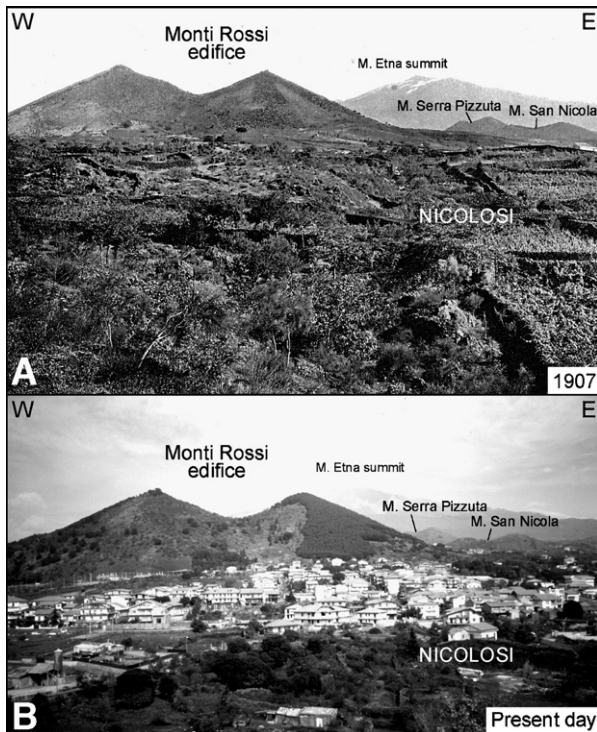


Fig. 9. Comparison between two photographs of Monti Rossi cone and Nicolosi village (A) at the beginning of the XX century (after De Lorenzo, 1907) and (B) at the present day: the populated area has extended greatly.

more than one breached crater, as in the cases of M. Gervasi, Cantone edifice (Fig. 3A, Fig. 8B) and M. Troina (Fig. 3A).

To quantify the orientation of this feature, the direction and azimuth of the ideal breaching-depression bisector, as indicated by red arrows in plan view (Fig. 3A), have been represented in a rose diagram as dip direction with 10-degree intervals (Fig. 7D). Two sets of breaching directions are evident. The first shows a dominant southward orientation ( $\pm 20^\circ$ ) and represents data from the central-western part of the studied area. The second set is mostly towards the SE ( $\pm 15^\circ$ ) and represents data from the eastern part of the studied area.

The above trends can be explained by differences in slope inclination in the two sectors. In the western and central part of the area, the trend is consistent with the evidence from other morphometric parameters that suggest N–S-striking fractures. Only lava flow paths are influenced by the gentle SE-dipping slope. In comparison, the slope in the extreme northeastern sector has an inclination up to  $20^\circ$  due to a hidden escarpment, which controls the emplacement and breaching of the cone regardless of the fracture orientation (Fig. 7B).

Other less well represented directions can be understood by considering an additional local control exerted by an already formed portion of the same multiple-edifice acting as a morphological obstacle. This is the case in northern M. Gervasi, which is breached to the WSW. Another example is the northern Cantone edifice, which is breached in the ESE direction (Fig. 8B).

## 5. Discussion and conclusions

The results provided by this work reveal a twofold application, which includes:

- (1) The suggestion of a methodology to analyse the relationship between parasitic pyroclastic cones and their substrate, and the proposal of a new morphological classification of cone typologies based on the parameterisation of the coeval eruption points along the same magma-feeding fracture.
- (2) Information on the upper Pleistocene–Holocene geological evolution and magma-feeding fracture system of a previously poorly understood portion of the southeastern flank of Mount Etna, and its relation to volcanic structures.

### 5.1. Cone types and their relations with the underlying fractures

This work suggests that monogenetic cones can range in type between two end-members, simple cones or multiple rifted edifices, with intermediate conditions (multiple superimposed, multiple coalescent or mixed types), which are distinguished and classified based on the observation of coeval eruption points (as indicated by craters) along the same magma-feeding fracture. We propose that two possible factors control the growth and evolution of a cone and its superficial eruptive conduit. These are the tectonic confining forces acting on the fracture in the substrate and the opposing magma supply pressure. The cone type (refer to Section 4.2) is determined by these two factors.

The emplacement of a simple cone (circular or elongated), grown around a single eruption point, can be related to a feeding fracture constrained by a relatively high confining stress in the substrate, or a low magma pressure. Both result in a localised eruptive conduit (Fig. 8A). The other end is a multiple rifted cone, which is a strongly elongated edifice formed along closely-spaced multiple eruption points. This type of cone could be related to a fracture constrained by a relatively low stress or a high magma pressure (Fig. 8C), both favouring

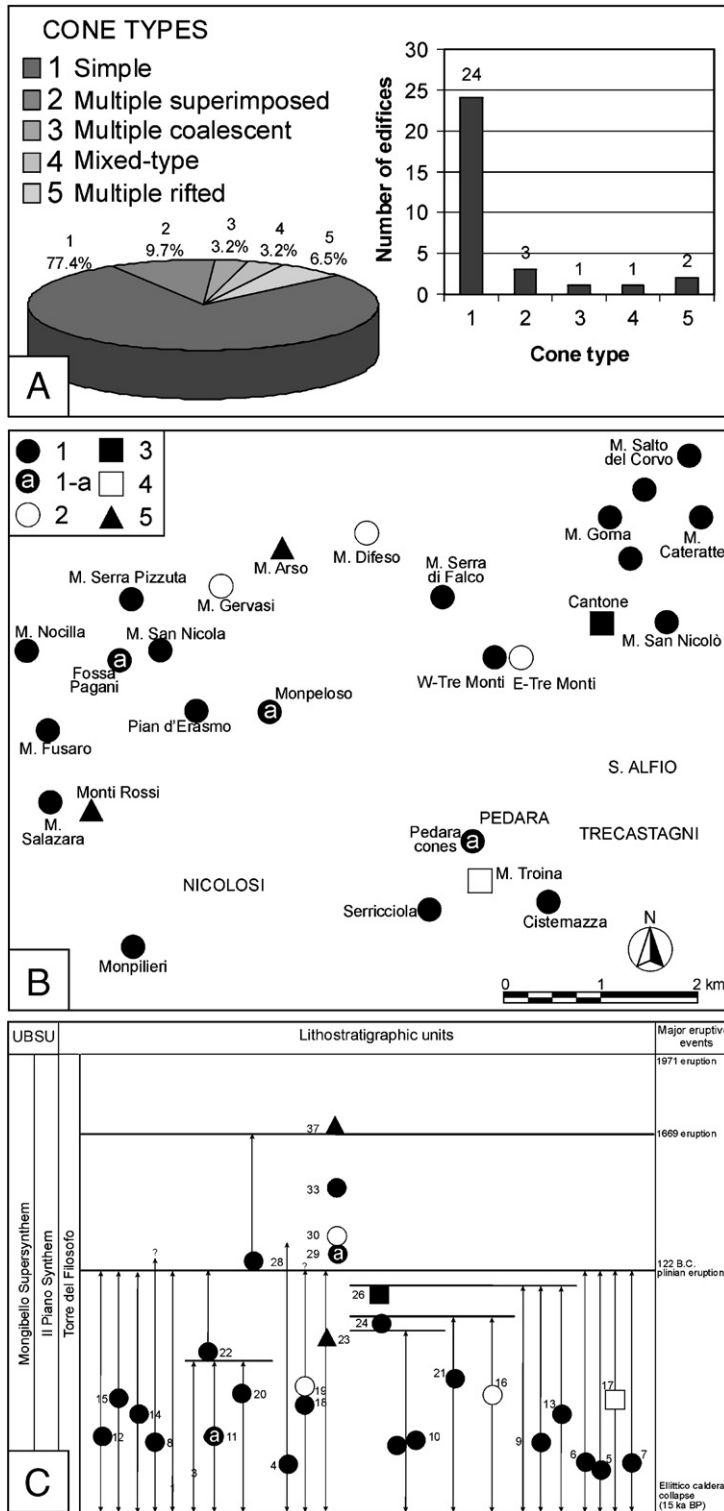


Fig. 10. (A) Cone type percentage in the population of studied cones. The most represented is the simple cone type (24 edifices, 77.4%), while the other types are represented by 1 to 3 edifices each (3.2% to 9.7%). Distribution of the different cone types with spatial (B) and relative age (C) position. Although the different types are not equally represented and type 1 predominates, no particular distributions in time or space are evident.

fracture opening. The other cone types, defined based on the distance between conduits, are generated by intermediate conditions. If there is constant confining stress acting in an area for a certain period, the formation of different cone types depends on locally variable magma pressure. In other cases, a combination of both magma pressure and magnitude of confining forces can influence cone growth.

The most represented among the studied population of cones is the simple cone type (24 edifices, 77.4%), while the other types are represented by a maximum of 3 edifices each (9.7%) (Fig. 10A). This means that it is more difficult to evaluate the statistical weight of typologies 2, 3, 4 and 5 than typology 1 in the study of spatial (Fig. 10B) or relative age (Fig. 10C) distribution. Nevertheless, it is reasonable to say that

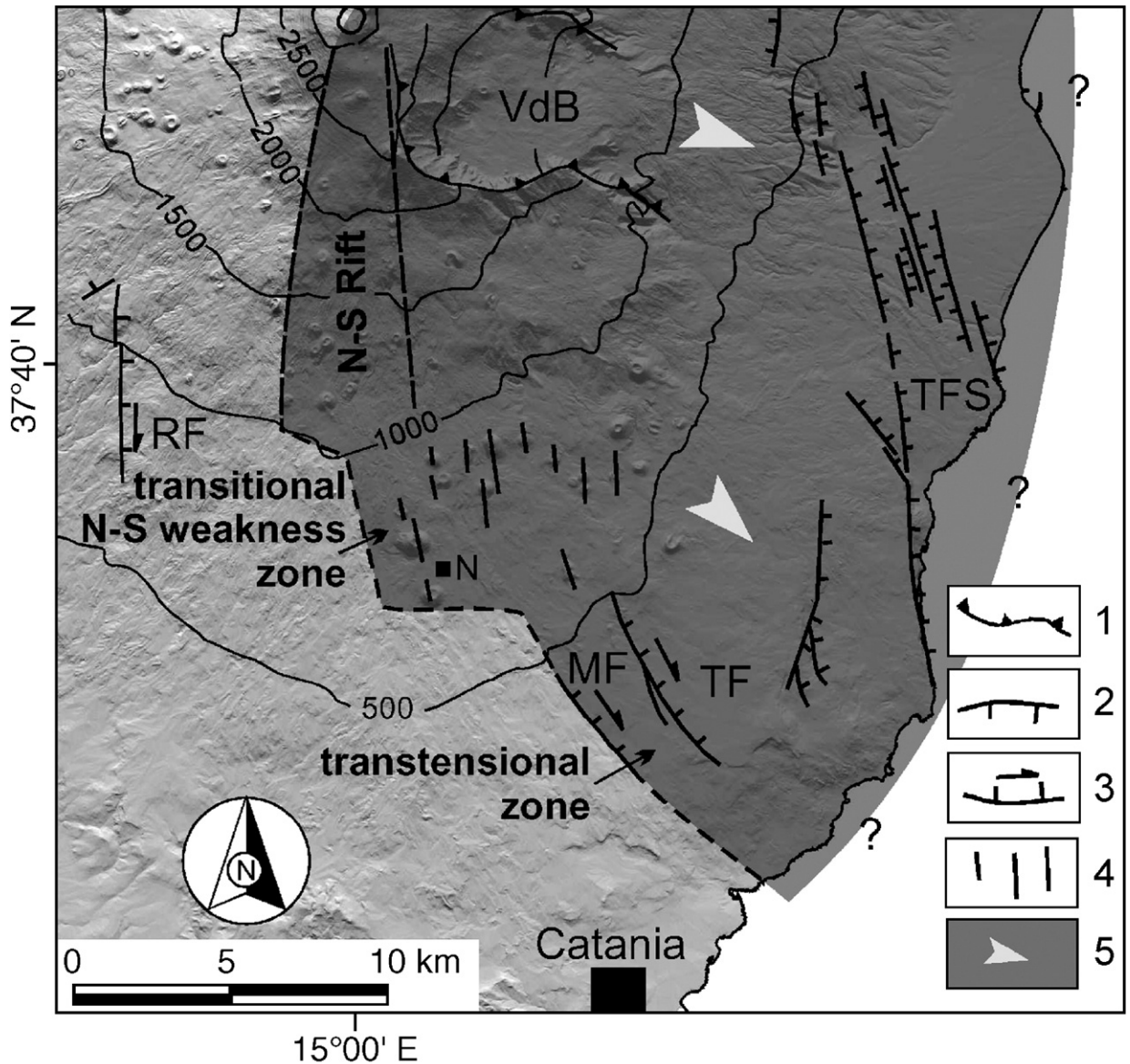


Fig. 11. The morphometric characteristics reflect the geometry of a N–S magma-feeding fracture field. The studied area can be regarded as a transitional weakness zone between the N–S Rift and the releasing system represented by the transtensional Trecastagni and Mascalucia faults, indicating a local component of extension oriented E–W, possibly related to the interplay between the regional Timpe fault system and the eastward gravitational spreading of the volcano. N, Nicolosi; VdB, Valle del Bove; TFS, Timpe Fault System; MF, Mascalucia Fault; TF, Trecastagni Fault; RF, Ragalna Fault. (1) Valle del Bove rim, (2) active normal fault, (3) active transtensional fault, (4) eruptive fractures, (5) displacement zone. Background shaded DEM after Pareschi et al. (1999), light from the north.

in the studied area no particular clustering of any cone type is evident both in space and time.

### 5.2. Reconstruction of the fracture field based on morphometric analysis

The application of the proposed methodology consists of a detailed morphometric analysis using accurate geological reconstruction. It is useful for indirectly assessing the magma-feeding structures in the substrate, which can be completely hidden by recent products at moderate altitudes on the southeastern slope of the volcano. Here only the paths of lava flows are influenced by the gentle and generally SE-dipping slope of the volcano, oblique to the prevailing direction of cone morphologic features. In places where the slope is steeper than  $10^\circ$ , as in the case of the extreme northeastern part of the studied area, is the influence of the fracture system outweighed by the control of the pre-existing topography on cone development. As a general application, the cone morphology and lava behaviour in different slopes can be useful in assessing the relative age of the substrate morphostructure given the stratigraphic position of the cone.

The results obtained agree with the suggestion of the existence of a magma-feeding fracture field in the studied area, which is dominated by approximately N–S-striking structures (blue traces in Fig. 3A; Fig. 11).

### 5.3. Relations with the structural framework of Mount Etna

The N–S Rift is interrupted at about 1100 m a.s.l., north of Nicolosi, where there is an eastward shift in the magma-feeding fracture zone of about 2 km. A wider weakness zone, characterised by the presence of numerous N–S-striking eruptive fractures in the investigated area, is observed down to an altitude of about 500 m. This weakness zone appears to interrupt in correspondence with the transtensional deformation represented by the Mascalucia and Trecastagni faults (Fig. 11). We consider that this Nicolosi weakness zone is not exactly the direct southwards extension of the N–S Rift, but rather a transition zone between the rift that ends at about 1100 m a.s.l. and the releasing system represented by the transtensional Trecastagni and Mascalucia faults. We suggest that this area indicates a local component of E–W extension. This is consistent with the present in-situ stress measurements of Bousquet and Lanzafame (2004). Such extension is possibly due to the interplay between the regional Timpe fault

system and the eastward gravitational spreading of the eastern flank of the volcano (Fig. 11).

These results are not in disagreement with Rust and Neri (1996) and Neri et al. (2004). The more western block between the Ragalna fault and the Trecastagni–Mascalucia system could be moving as well, although more slowly with respect to the eastern zone.

The proposed methodological approach does not supply direct information on the state of stress of a region. It only gives information on the magma-feeding fracture geometry. In light of the observations described in the foregoing, it is not possible to exclude oblique displacements accompanying the N–S-striking eruptive fractures within the studied area.

### Acknowledgments

This research was partially supported by a FIRB–MIUR project (n. RBAU01LHEE) to A.T., and was done in the framework of the ILP project entitled “New tectonic causes of volcano failure and possible premonitory signals” and of the UNESCO–IUGS–IGCP projects no. 455 “Basement Volcanoes Interplay and Human Activities” and no. 508 “Volcano collapse and fault activity”. G. Pasquaré and S. Branca are acknowledged for field cooperation, and C.C. expresses her gratitude to N. and M. Arcidiacono for their hospitality and logistical support. We wish to thank J.W. Head III and D.J. Rust for their careful reviews and suggestions on an earlier version of the manuscript.

### References

- Acocella, V., Neri, M., 2003. What makes flank eruptions? The 2001 Etna eruption and its possible triggering mechanisms. *Bull. Volcanol.* 65 (7), 517–529.
- Azzaro, R., 2004. Seismicity and active tectonics in the Etna region: constraints for a seismotectonic model. In: Bonaccorso, A., Calvari, S., Coltelli, M., Del Negro, C., Falsaperla, S. (Eds.), *Mt. Etna: Volcano Laboratory*. AGU Geophys. Monogr., vol. 143, pp. 205–220.
- Borgia, A., Ferrari, L., Pasquaré, G., 1992. Importance of gravitational spreading in the tectonic and volcanic evolution of Mount Etna. *Nature* 357, 231–235.
- Bousquet, J.C., Lanzafame, G., 2004. The tectonics and geodynamics of Mt. Etna: synthesis and interpretation of geological and geophysical data. In: Bonaccorso, A., Calvari, S., Coltelli, M., Del Negro, C., Falsaperla, S. (Eds.), *Mt. Etna: Volcano Laboratory*. AGU Geophys. Monogr., vol. 143, pp. 29–48.
- Branca, S., Coltelli, M., Groppelli, G., 2004. Geological evolution of Etna volcano. In: Bonaccorso, A., Calvari, S., Coltelli, M., Del Negro, C., Falsaperla, S. (Eds.), *Mt. Etna: Volcano Laboratory*. AGU Geophys. Monogr., vol. 143, pp. 49–64.
- Branca, S., Del Carlo, P., 2004. Eruptions of Mt. Etna during the past 3,200 years: a revised compilation integrating the historical and stratigraphic record. In: Bonaccorso, A., Calvari, S., Coltelli, M.,

- Del Negro, C., Falsaperla, S. (Eds.), Mt. Etna: Volcano Laboratory. AGU Geophys. Monogr., vol. 143, pp. 1–28.
- Branca, S., Del Carlo, P., 2005. Types of eruptions of Etna volcano. *Bull. Volcanol.* 67, 732–742. doi:10.1007/s00445-005-0412-z.
- Calvari, S., Tanner, L.H., Groppelli, G., Norini, G., 2004. Valle del Bove, eastern flank of Etna volcano: a comprehensive model for the opening of the depression and implications for future hazards. In: Bonaccorso, A., Calvari, S., Coltelli, M., Del Negro, C., Falsaperla, S. (Eds.), Mt. Etna: Volcano Laboratory. AGU Geophys. Monogr., vol. 143, pp. 65–75.
- Chester, D.K., Duncan, A.M., Guest, J.E., Kilburn, C.J.R., 1985. Mount Etna: the Anatomy of a Volcano. Chapman and Hall, London. 404 pp.
- Coltelli, M., Del Carlo, P., Vezzoli, L., 1998. Discovery of a plinian basaltic eruption of Roman age at Etna volcano, Italy. *Geology* 26 (12), 1095–1098.
- De Lorenzo, G., 1907. L'Etna. Con 150 illustrazioni e 3 tavole. Collezione di monografie illustrate: serie I. Italia artistica, 36. Istituto Italiano d'Arti Grafiche Ed., Bergamo.
- Del Carlo, P., Branca, S., 1998. Tephrostratigraphic dating of the pre-1300 AD SE flank eruptions of Mt. Etna. *Acta Vulcanologica* 10 (1), 33–37.
- Del Carlo, P., Vezzoli, L., Coltelli, M., 2004. Last 100 ka tephrostratigraphic record of Mount Etna. In: Bonaccorso, A., Calvari, S., Coltelli, M., Del Negro, C., Falsaperla, S. (Eds.), Mt. Etna: Volcano Laboratory. AGU Geophys. Monogr., vol. 143, pp. 77–89.
- Favalli, M., Innocenti, F., Pareschi, M.T., Pasquaré, G., Branca, S., Cavarra, L., Mazzarini, F., Tibaldi, A., 1998. The DEM of Mt. Etna: geomorphologic and structural implications. *Geodin. Acta* 12 (5), 279–290.
- Ferrari, L., Tibaldi, A., 1991. I coni avventizi dell'Etna: influenza della geometria delle discontinuità sulla crescita degli apparati vulcanici. *Resoconti Conv. Soc. Geol. It., Giornate in Memoria di Leo Ogniben. Naxos, Italia, 6–8 June 1991*, pp. 212–213.
- Foglio 625 Acireale, in press. Servizio Geologico d'Italia, Carta Geologica d'Italia alla scala 1:50.000, Roma.
- Froger, J.L., Merle, O., Briole, P., 2001. Active spreading and regional extension at Mount Etna imaged by SAR interferometry. *Earth Planet. Sci. Lett.* 187, 245–258.
- Hasenaka, T., Carmichael, I.S.E., 1985. The cinder cones of Michoacan–Guanajuato, central Mexico: their age, volume and distribution, and magma discharge rate. *J. Volcanol. Geotherm. Res.* 25, 104–124.
- Johnson, C.A., Harrison, C.G.A., 1990. Neotectonics in central Mexico. *Phys. Earth Planet. Inter.* 64, 187–210.
- Lo Giudice, E., Rasà, R., 1992. Very shallow earthquakes and brittle deformation in active volcanic areas: the Etna region as an example. *Tectonophysics* 202, 257–268.
- Mazzarini, F., Armienti, P., 2001. Flank cones at Mount Etna volcano: do they have a power-law distribution? *Bull. Volcanol.* 62, 420–430.
- McGuire, W.J., Pullen, A.D., 1989. Location and orientation of eruptive fissures and feeder-dykes at Mount Etna: influence of gravitational and regional stress regimes. *J. Volcanol. Geotherm. Res.* 38, 244–325.
- Nakamura, K., 1977. Volcanoes as possible indicators of tectonic stress orientation — principles and proposal. *J. Volcanol. Geotherm. Res.* 2, 1–16.
- Neri, M., Acocella, V., Behncke, B., 2004. The role of the Pernicana Fault System in the spreading of Mt. Etna (Italy) during the 2002–2003 eruption. *Bull. Volcanol.* 66, 417–430.
- Ollier, C., 1988. Volcanoes. Basil Blackwell, New York.
- Pareschi, M.T., Cavarra, L., Favalli, M., Innocenti, F., Mazzarini, F., Pasquaré, G., 1999. Digital atlas of the Mt. Etna volcano. *Acta Vulcanologica* 11 (2), 311–314 CD-ROM provided.
- Pasquaré, G., Tibaldi, A., Attolini, C., Cecconi, G., 1988. Morphometry, spatial distribution and tectonic control of Quaternary volcanoes in northern Michoacan, Mexico. *Rend. Soc. Ital. Mineral. Petrol.* 43 (4), 1215–1225.
- Patané, D., De Gori, P., Chiarabba, C., Bonaccorso, A., 2003. Magma ascent and the pressurization of Mount Etna's volcanic system. *Science* 299, 2061–2063.
- Porter, S.C., 1972. Distribution, morphology and size frequency of cinder cones on Mauna Kea volcano, Hawaii. *Geol. Soc. Amer. Bull.* 83, 3607–3612.
- Romano, R., Sturiale, C., 1982. The historical eruptions of Mt. Etna (volcanological data). *Mem. Soc. Geol. Ital.* 23, 75–97.
- Romano, R., Sturiale, C., 1981. Geologia del versante sud-orientale etneo, F° 270 IV (NO, NE, SO, SE). *Boll. Soc. Geol. Ital.* 100, 15–40.
- Rust, D., Neri, M., 1996. The boundaries of large-scale collapse on the flanks of mount Etna, Sicily. In: Neuberg, J. (Ed.), *Volcano Instability on the Earth and Other Planets*. *Geol. Soc. Spec. Publ.*, vol. 110, pp. 193–208.
- Settle, M., 1979. The structure and emplacement of cinder cone fields. *Am. J. Sci.* 279, 1089–1107.
- Strecker, M., Bosworth, W., 1991. Quaternary stress-field change in the Gregory Rift, Kenya. *Eos Trans., AGU* 72, 17–22.
- Tibaldi, A., Groppelli, G., 2002. Volcano-tectonic activity along the structures of the unstable NE flank of Mt. Etna, Italy. *J. Volcanol. Geotherm. Res.* 115 (3–4), 277–302.
- Tibaldi, A., 1995. Morphology of pyroclastic cones and tectonics. *J. Geophys. Res.* 100 (B12), 24521–24535.
- Tibaldi, A., Civelli, G., Pecchio, M., 1989. Tectonic control on morphometry of cinder cones in Lanzarote and Fuerteventura, Canary Islands. *Proceedings of the International Meeting on Canarian Volcanism, Lanzarote, Canary Islands*. European Science Foundation, pp. 216–219.
- Villari, L., Rasà, R., Callano, A., 1988. Considerazioni sull'hazard vulcanico e sul campo di sforzi della regione etnea attraverso l'analisi morfometrica e la distribuzione piano altimetrica dei cono avventizi. *Boll. GNV IV*, 600–619.
- Wood, C.A., 1980. Morphometric evolution of cinder cones. *J. Volcanol. Geotherm. Res.* 7, 387–413.